Article

Multi-Response Optimization of Abrasive Waterjet Cutting on r-GO-Reinforced Fibre Intermetallic Laminates through Moth–Flame Optimization Algorithm

Devaraj Rajamani [1,*], Mahalingam Siva Kumar [1] and Esakki Balasubramanian [2]

[1] Centre for Advanced Materials Processing, Department of Mechanical Engineering, Vel Tech Rangarajan Dr. Sagunthala R&D Institute of Science and Technology, Chennai 600062, India; drmsivakumar@veltech.edu.in
[2] Department of Mechanical Engineering, National Institute of Technical Teachers Training and Research, Chennai 600113, India; esak.bala@gmail.com
* Correspondence: rajamanitamil1991@gmail.com

Abstract: Laminated metal-composite structures, also known as fibre metal laminates (FMLs), have emerged as prominent engineering materials in various industries, particularly in the domains of aircraft and automobile manufacturing. These materials are sought after due to their enhanced impact and fatigue resistance capabilities. The machining of FMLs plays a crucial role in achieving near-net shapes for the purpose of joining and assembling components. Delamination is a prevalent issue encountered during the process of conventional machining, thus rendering FMLs are challenging materials to machine. This study aims to investigate the cutting process of novel fibre intermetallic laminates (FILs) using the abrasive water jet (AWJ) cutting technique. The FILs consists of carbon and aramid fibers that are adhesively bonded with a resin matrix filled with reduced graphene oxide (r-GO) nano fillers. Moreover, these laminates contain embedded Nitinol shape memory alloy sheets as the skin materials. Specifically, the study aims to investigate the impact of different factors, such as the addition of reduced graphene oxide (r-GO) in the laminates (ranging from 0 to 2 wt%), traverse speed (ranging from 400 to 600 mm/min), waterjet pressure (ranging from 200 to 300 MPa), and nozzle height (ranging from 2 to 4 mm), on the material removal rate (MRR), delamination factor (FD), and kerf deviation (KD). ANOVA was used in the statistical analysis to determine the most influential parameters and their effects on the selected responses. The optimal AWJC parameters are determined using a metaheuristic-based moth–flame optimization (MFO) algorithm in order to enhance cut quality. The efficacy of MFO is subsequently compared with similar well-established metaheuristics such as the genetic algorithm, particle swarm algorithm, dragonfly algorithm, and grey-wolf algorithm. MFO was found to outperform in terms of several performance indices, including rapid divergence, diversity, spacing, and hypervolume values, among the algorithms compared.

Keywords: fibre metal laminates; optimization; metaheuristics; moth–flame optimization; statistical analysis; abrasive waterjet cutting

1. Introduction

Fibre metal laminates, often known as FMLs, are a pioneering kind of advanced composite material that has spurred a revolution in the use of composite materials in aerospace and structural engineering applications. FMLs have emerged as a viable alternative to fulfil the ever-growing need for lightweight, high-strength materials [1]. By combining the great mechanical capabilities of both metal alloys and high-performance fibers, FMLs have been able to combine the exceptional mechanical properties of both types of materials. The mechanical properties of FMLs are considerably improved with the addition of nano fillers into the polymer matrix materials. Recently, several researchers have studied the

impact of incorporating nano fillers such as nano clay, carbon nano tubes (CNTs), titanium oxide (TiO_2), graphene oxides (GO and r-GO), and silicon oxide (SiO_2), and their concentrations, on the mechanical properties of FMLs. Among the various nano fillers, reduced graphene oxide (r-GO), a novel two-dimensional derived member of nanocarbon, has gained significant attention from researchers due to its outstanding properties, such as higher surface area, exceptional elastic modulus, and improved electrical conductivity [2–4]. Because of the one-of-a-kind synergy that exists between metallic layers and fibre-reinforced composites, FMLs provide a harmonic balance of stiffness, strength, and damage tolerance. As a result, FMLs are very helpful in a variety of important sectors [5]. The inherent complexity of FMLs results in a challenging set of problems that must be overcome before FMLs can be considered successful for end-use applications. One of the most significant obstacles is the heterogeneity of FMLs, which occurs when alternating layers of metal and fibre-reinforced composites display significantly different mechanical characteristics. This heterogeneity frequently leads to concerns such as differential wear on cutting tools and uneven material removal rates, both of which may impact the dimensional accuracy of machined components [6]. Furthermore, the abrasive nature of the reinforcing fibers inside FMLs may result in quick tool wear and delamination, which poses substantial challenges to obtaining the necessary surface finish and limiting damage to the material. As FMLs continue to gain popularity in aerospace and structural applications, a more in-depth knowledge of these machining issues becomes important. This drives the need for creative machining processes and tactics to unleash the full potential of these sophisticated materials [7].

Abrasive waterjet (AWJ) machining has emerged as a promising unconventional machining process for the precise shaping and trimming of FMLs. FMLs consist of alternating layers of metal and fibre-reinforced composites, requiring machining processes that can effectively minimize delamination and fibre damage while preserving the structural integrity of the metallic layers. AWJ machining, known for its non-thermal and non-contact characteristics, has demonstrated significant advantages, such as precision and versatility for intricate designs and shapes, which reduce the need for secondary finishing processes. Additionally, it is environmentally friendly, as it produces minimal waste and does not emit harmful fumes or gases, setting it apart as a sustainable choice for modern manufacturing when compared with other non-traditional machining processes. By utilizing a high-velocity flow of water mixed with abrasive particles, AWJ machining enables precise cutting and trimming of FMLs while minimizing the formation of heat-affected zones and reducing the risk of mechanical damage [8]. The versatility of this technique allows for the machining of intricate geometries with exceptional accuracy, making it highly suitable for the complex structures and architectures commonly encountered in FMLs. On the other hand, achieving effective cut quality characteristics in AWJ cutting of novel engineering materials, especially in stacked composite laminates, is still difficult due to the abundance of process related variables and the dominance of quality deficiencies such as delamination, fibre pull-out, a higher kerf ratio, and inferior surface quality [9]. Therefore, in order to achieve defect-free components that fulfil functional requirements, particularly for FMLs, it is necessary to conduct in-depth research into the effects of AWJ cutting parameters on these response properties.

In the recent past, several researchers have extensively investigated the impact of AWJ cutting on composite laminates. The AWJ cutting characteristics of a composite consisting of lanthanum phosphate and yttria were investigated by K. Balamurugan et al. [10] using a response surface approach. The impacts of kerf taper, surface quality, and material removal rate, along with cutting speed, stand-off distance, and water pressure, have been taken into consideration as input factors. The results of their study indicate that the cutting speed has a detrimental effect on surface quality, while water pressure has a beneficial effect on both kerf taper and material removal rate. The effects of significant parameters of AWJ cutting on the kerf taper and surface roughness of a hybrid composite made of glass and coconut fibre were investigated by Kalirasu et al. [11] using the Taguchi methodology. Based on the findings of

the investigation, it can be concluded that the chosen response characteristics are primarily influenced by the size of the abrasive particles. Alberdi et al. [12] conducted a drilling operation through AWJ machining on Ti/CFRP stacked composite laminates to investigate their qualitative traits. The research findings indicate that the arrangement of stacks, water pressure, and traverse speed of the focusing tube play a crucial role in determining the taper of drilling and surface quality. Hutyrová et al. [13] conducted an experimental investigation to examine the surface topography of wood plastic composites machined using AWJ. Based on their findings, the utilization of AWJ cutting was determined to be an effective method for machining plastic composites while avoiding the melting of the matrix materials. Kalirasu et al. [14] employed an analytical technique known as response surface methodology (RSM) and multi-objective optimization based on ratio analysis (MOORA) to evaluate the performance of jute/polyester composites in terms of AWJ cutting assessment. An investigation was conducted to examine the impact of stand-off distance, cutting speed, and jet pressure on the kerf taper and surface roughness of machined surfaces. The results indicate that the proposed method is capable of effectively handling fibre-reinforced composites with a maximum thickness of 3 mm. Pahuja et al. [15] conducted experimental and statistical analyses to investigate the surface and kerf characteristics of stacked titanium (Ti) and carbon fibre reinforced polymer (CFRP) fibre metal laminates (FMLs) using AWJ cutting. It has been asserted that the uppermost layer of the skin is the site where micro buckling and fractures initiate the erosion mechanism of FMLs. Furthermore, the influence of the metal skin and polymer composite designs on the failures of the FML interface is significant. Ramulu [16] conducted an analytical investigation of the influence of AWJ cutting factors on the kerf quality of machined Ti/CFRP composite stacks. An empirical model was developed to predict the depth of penetration and material removal mechanism resulting from water jet pressure. It was found that this model can effectively guide the adjustment of parameters in AWJ cutting to achieve defect-free cutting zones. However, only a few research studies are available on the multi-response optimization of AWJ cutting on FMLs, especially when adopting metaheuristic algorithms.

This study focuses on the analysis of the AWJ cutting capabilities of a newly developed fibre intermetallic laminate (FIL). The FIL is composed of reduced graphene oxide (r-GO)-filled epoxy prepregs, which are reinforced with a combination of carbon and aramid fibres. Additionally, Nitinol shape memory alloy sheets are incorporated as the skin materials in the FIL structure. The independent variables considered in this research include traverse speed, waterjet pressure, and nozzle height, along with different wt% values of r-GO nano fillers. The influence of these independent variables on three response characteristics, namely material removal rate, delamination factor, and kerf deviation, were investigated through statistical analysis and response surface plots. A metaheuristic-based moth–flame optimization (MFO) algorithm was used to optimize the AWJ cutting parameters to improve the cut quality features, with its results compared to those of other, more well-known metaheuristic algorithms, such as the genetic algorithm (GA), particle swarm algorithm (PSO), grey-wolf algorithm (GWO), and dragonfly algorithm (DFO).

2. Methodologies

2.1. Response Surface Methodology

This study investigates the effects of selected AWJ cutting variables and the incorporation of r-GO in FILs on selected quality and performance characteristics including *MRR*, *FD*, and *KD*. Since there are numerous process-related parameters that are dynamically engaged in the material removal mechanism, the AWJ cutting process has become exceedingly complicated. Thus, the experimentation and prediction of optimal process variables requires a viable and systematic experimental plan in order to minimize the number of experimental trials, and thereby reduce processing costs and time consumption. Response surface methodology (RSM) has been found to be an effective technique for designing experiments with a minimum number of experimental trials in order to determine the interaction between dependent and predictor variables of complex processes such as machining, additive

manufacturing, and thermo-mechanical systems [17]. In order to construct higher-order mathematical models for optimization, the current study employs Box–Behnken design (BBD), a subset of RSM, to design and conduct AWJ cutting experiments. The formulation of quadratic polynomial models by means of RSM is as follows:

$$R = \beta_0 \sum_{i=1}^{k} \beta_i x_i + \sum_{i=1}^{k} \beta_{ii} x_i^2 + \sum_i \sum_j \beta_{ij} x_i x_j + \varepsilon \tag{1}$$

where R is the response and x_i is the value of the ith AWJ cutting parameter; β_0 is the model constant; β_i, β_{ij}, β_{ii} represent the linear, interaction, and quadratic coefficients, respectively; and ε indicates the statistical distribution error. The relevant data are typically acquired through the design of experiments, followed by the statistical multiple regression approach, to develop the empirical models. To explain the relevance of the empirical model, a more popular statistical method such as analysis of variance (ANOVA) is used.

2.2. Moth–Flame Optimization Algorithm

The moth–flame optimization (MFO) algorithm is a novel stochastic population-based approach which is primarily inspired by moths' natural transverse orientation navigational strategy [18]. Moths can only migrate in a straight line using this strategy when the light source is far away. The moth's objective is to get to the flame. The flame's objective is to achieve its ideal location and improve flame density. According to the flowchart shown in Figure 1, MFO begins by creating moths at random in the solution space, calculates each moth's fitness values (i.e., location), and tags the ideal position with a flame. The next step is to update the moths' positions using a spiral movement function to obtain better positions that are tagged by a flame, update the new best individual positions, and then repeat the previous steps (updating the moths' positions and generating new positions) until the termination criteria are satisfied.

The overall structure of the MFO algorithm consists of three stages, namely initialization, iteration, and the stopping criterion. The step-by-step implementation of MFO algorithms is as follows:

2.2.1. Stage 1: Initializing the Population of Moths

The location of the moth in space must be solved as a variable in the MFO algorithm, which assumes that the moth represents a potential solution to the considered problem. Moths can fly in one, two, three, and hyperdimensional space by modifying their position vectors. Given that MFO is basically a swarm intelligence optimization technique, the moth population can be represented as follows:

$$M = \begin{bmatrix} m_{11} & m_{12} & \cdots & \cdots m_{1d} \\ m_{21} & m_{22} & \cdots & \cdots m_{2d} \\ \vdots & \vdots & \vdots & \vdots & \vdots \\ m_{n1} & m_{n2} & \cdots & \cdots m_{nd} \end{bmatrix} \tag{2}$$

where the number of moths can be denoted as n and the number of process parameters (dimensions of the problem) can be represented as d. The corresponding fitness values for the selected number of moths can be represented and memorized in an array as follows:

$$OM = \begin{bmatrix} Om_1 \\ Om_2 \\ \vdots \\ Om_n \end{bmatrix} \tag{3}$$

where the fitness function value of the corresponding moth is denoted as Om_i, which is determined according to the actual situation.
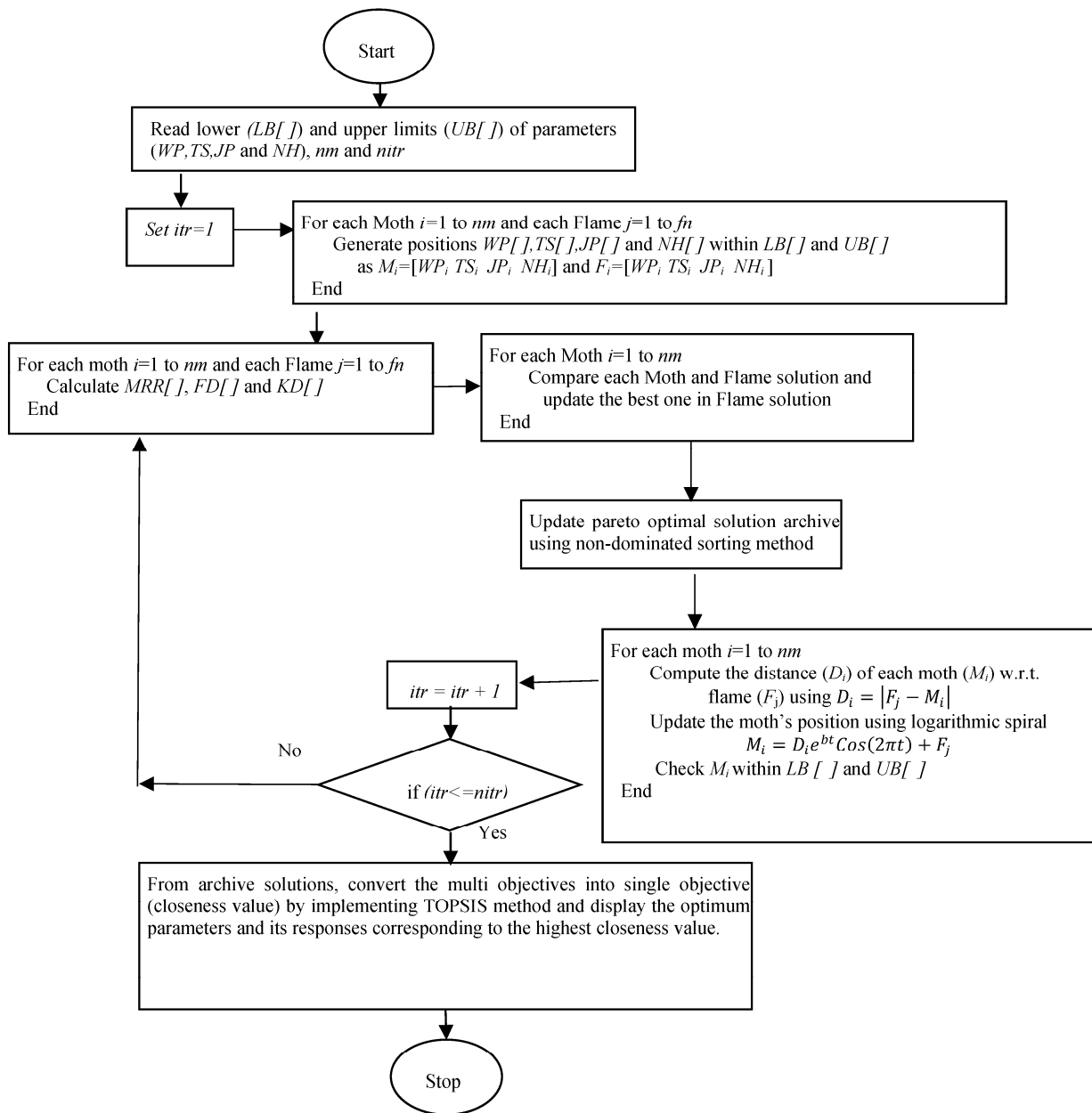
```
                                    ┌─────────┐
                                    │  Start  │
                                    └─────────┘
```

Read lower *(LB[ ])* and upper limits *(UB[ ])* of parameters
(WP,TS,JP and *NH), nm* and *nitr*

Set itr=1

For each Moth *i*=1 to *nm* and each Flame *j*=1 to *fn*
    Generate positions *WP[ ],TS[ ],JP[ ]* and *NH[ ]* within *LB[ ]* and *UB[ ]*
        as M_i=[WP_i TS_i JP_i NH_i] and F_i=[WP_i TS_i JP_i NH_i]
End

For each moth *i*=1 to *nm* and each Flame *j*=1 to *fn*
    Calculate *MRR[ ], FD[ ]* and *KD[ ]*
End

For each Moth *i*=1 to *nm*
    Compare each Moth and Flame solution and
        update the best one in Flame solution
End

Update pareto optimal solution archive
using non-dominated sorting method

For each moth *i*=1 to *nm*
    Compute the distance (D_i) of each moth (M_i) w.r.t.
        flame (F_j) using $D_i = |F_j - M_i|$
    Update the moth's position using logarithmic spiral
        $M_i = D_i e^{bt} Cos(2\pi t) + F_j$
    Check M_i within *LB [ ]* and *UB[ ]*
End

itr = itr + 1

if *(itr<=nitr)*

No

Yes

From archive solutions, convert the multi objectives into single objective
(closeness value) by implementing TOPSIS method and display the optimum
parameters and its responses corresponding to the highest closeness value.

```
                                    ┌─────────┐
                                    │  Stop   │
                                    └─────────┘
```

Figure 1. Flowchart for the execution of the MFO algorithm.

The remaining elements in MFO are flames, which can be denoted in *D*-dimensional space as a matrix [*F*] followed by its fitness function vector [*OF*].

$$F = \begin{bmatrix} f_{11} & f_{12} & \cdots & \cdots f_{1d} \\ f_{21} & f_{22} & \cdots & \cdots f_{2d} \\ \vdots & \vdots & \vdots & \vdots \vdots \\ f_{n1} & f_{n2} & \cdots & \cdots f_{nd} \end{bmatrix} \qquad (4)$$

$$OF = \begin{bmatrix} Of_1 \\ Of_2 \\ \vdots \\ Of_n \end{bmatrix} \qquad (5)$$

It must be noted that the MFO algorithm provides solutions for both moths and flames. The way they are handled and updated in each iteration is what makes them different from one another. The moths are the real searchers; they travel around the search area, and their current best position is among the flames. In other words, flames may be thought of as flags or pins that moths drop while scouring the search area. In order to update a flag (flame) if a better solution is discovered, each moth examines the area surrounding it. A moth never loses its ideal solution with this process.

2.2.2. Stage 2: Updating the Position of Moths

To obtain the global optimal solutions of the optimization problems, MFO uses three distinct functions. The following is a definition of these functions:

$$MFO = (I, P, T) \tag{6}$$

where I indicates the first random locations of the moths, P indicates the movement of the moths in the search area, T indicates the end of the search process. The populations of MFO are initialized as follows:

$$M(i, j) = (u(i) - l(j)) \times (rand() + l(i)) \tag{7}$$

where the upper and lower bounds of the algorithm parameters are defined as $u \& l$, respectively. The moths fly in a transverse direction in the search area, as was previously indicated. When using a logarithmic spiral, the following three requirements must be met:

- The initial point of the spiral should start from the moth;
- The end point of the spiral should be at the position of the flame;
- The movement of the spiral should not exceed the search space.

To fulfil the above conditions, the logarithmic spiral for the MFO algorithm can be defines as follows:

$$S(M_i, F_j) = D_i . e^{bt} . \cos(2\pi t) + F_j \tag{8}$$

where the distance between the moth and flame $(|F_j - M_i|)$ is defined by D_i, the shape of the logarithmic spiral is denoted by b, and a random number between -1 to 1 is defined by t. The spiraling motion of the moth towards the flame in the search space ensures that exploitation and exploration are balanced in MFO. Furthermore, utilizing the OF and OM matrices, the moths fly around the flames (i.e., each moth flies encircling the closest flame) in order to avoid the probability of obtaining a local optimum.

2.2.3. Stage 3: Updating the Number of flames

The number of flames should be less during the iteration for obtaining the global optimal solutions. Hence, an adaptive mechanism has been selected for enhancing the exploitation of the MFO algorithm by simultaneously reducing the number of flames. The mathematical expression for updating the number of flames can be represented as follows:

$$f_{No} = round\left((N - l) \times \left(\frac{N - l}{T} \right) \right) \tag{9}$$

where the maximum number of flames can be represented as N, and the present iteration number and the maximum number of iterations are denoted as l and T, respectively.

3. Experimentation and Measurements

3.1. Fabrication of Fibre Intermetallic Laminates

The AWJ cutting experiments were conducted using FILs. These laminates were composed of Nitinol foils as the skin materials, epoxy resin as the matrix, and carbon/Kevlar as the prepreg materials. To fabricate these laminates, a vacuum-assisted resin infusion process was employed. Three different weight percentages of r-GO nano fillers (0%, 1%,

and 2%) were incorporated into the laminates. The r-GO fillers with varying weight percentages were evenly distributed into the acetone-diluted epoxy resin using mechanical stirring. The stirring process lasted for approximately 15 min at a probe speed of 120 rpm. To achieve a homogeneous mixture, a sonication process was conducted using an ultrasonic bath (Model: Sonoplus HD 2000, manufactured by Bandelin Electronic GmbH & Co. KG, Germany). The process lasted for a duration of 45 min, with a power output of 70 W. The temperature of resin and r-GO mixtures was reduced during the sonication process by placing the vessel in an ice water bath. Following the sonication process, the acetone present in the resin mixture was removed by subjecting the mixture to heat in a vacuum oven at a temperature of 70 °C for a duration of 60 min. The hardener was combined with the resin in a ratio of 10:1 using a magnetic stirrer set at a stirring speed of 180 rpm for a duration of 15 min. This process ensures improved dispersion of r-GO particles and the removal of any trapped air voids within the mixture. The r-GO-reinforced FILs were produced using a vacuum-assisted resin infusion process. This involves stacking woven carbon and aramid fibers in an alternating pattern, with two layers of outer-skinned Nitinol foils. The stacking sequence is as follows: NiTi/[carbon/epoxy/aramid]8/NiTi. The fabricated laminates underwent a curing process at an ambient temperature for a duration of 24 h, while being subjected to a pressure of 6 bar. The fabricated FIL had cross-sectional dimensions of $300 \times 300 \times 3.5 \pm 0.3$ mm^3.

3.2. Abrasive Waterjet Cutting of FILs

Using a high-precision cantilever type computer-numerical-controlled AWJ cutting machine (Model: S3015, Waterjet Germany, India), the cutting experiments were carried out on three different kinds of FILs made with 0, 1, and 2 wt% of r-GO nano fillers. To facilitate effective machining operations, the AWJ machine was outfitted with a high-pressure intensifier pump with an operating pressure of up to 450 MPa and a 0.76 mm diameter carbide nozzle. Throughout the studies, the machining parameters, including the abrasive flow rate of 200 g/min, the abrasive particle size of 177 μm, and the jet impact angle of 90°, were held constant. For the investigation of material removal rate, delamination factor, and kerf deviation, a total of 29 straight parallel slots with a cutting length of 50 mm were made in the various FILs in accordance with the RSM-BBD experimental design strategy for four dependent variables with three levels (Table 1). Figure 2 illustrates the AWJC experimental setup and the processed FIL samples. The AWJ cutting system has many process-related dependent variables, but the most important ones, such *TS*, *WP*, and *NH*, were chosen for the present study, and were obtained from exhaustive pilot studies based on the capability of the system and the available existing studies. Following the execution of the AWJ cutting experiments, the response variables *MRR*, *FD*, and *KD* were measured three times for each cut, and their mean values were considered for further studies to eliminate the statistical prediction errors. *MRR* represents the mass loss of substrate material during each experimental run and is calculated as follows:

$$MRR(g/s) = \left(\frac{Material\ removal\ for\ each\ cut \times cutting\ speed}{Length\ of\ cut} \right) \tag{10}$$

Table 1. Process parameters for AWJ cutting experimentation.

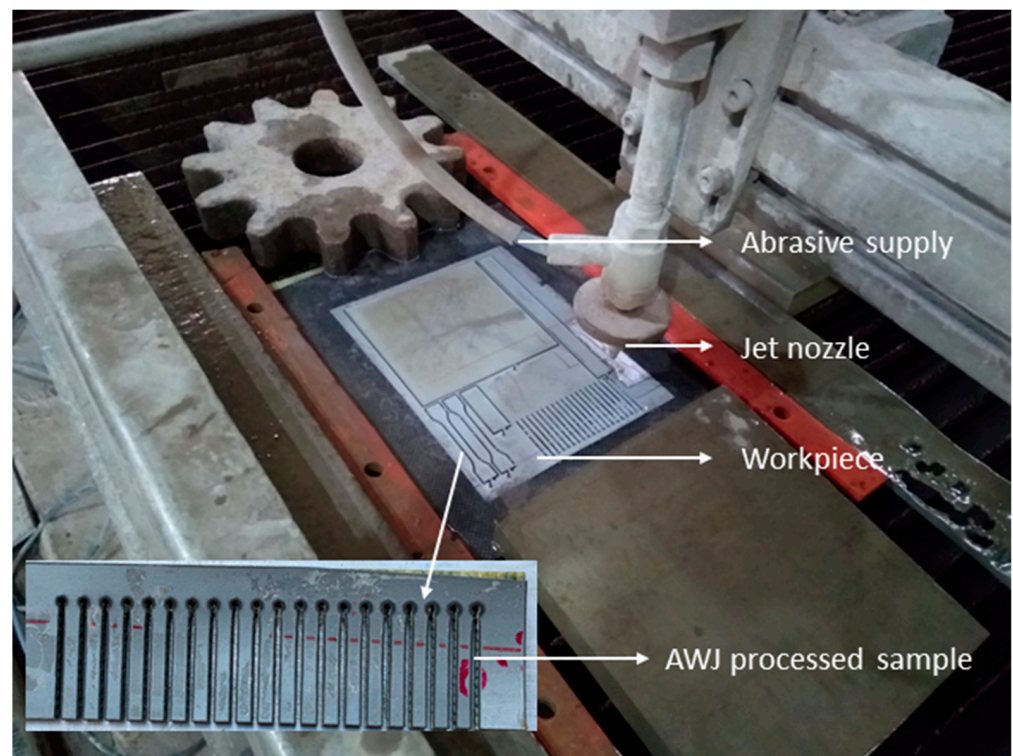| S. No.	Dependent Variables	Code	Levels		
			Low	Medium	High
1	Weight percentage of r-GO (wt%)	*r-GO*	0	1	2
2	Traverse speed (mm/min)	*TS*	400	500	600
3	Waterjet Pressure (MPa)	*WP*	200	250	300
4	Nozzle height (mm)	*NH*	2	3	4

Figure 2. Abrasive waterjet cutting on fabricated fibre intermetallic laminates.

A video measuring system (made by Accurate Gauge, India) outfitted with a high-resolution scanning system and M2-2D software was used to measure the delamination factor (*FD*), which is defined as the peel-up and push-out delamination along the slot of through cuts. The ratio between the maximum width of the delaminated area and the actual width of the cut along its length is used to calculate the delamination factor. The top kerf width of the cut surface was measured using a table top co-ordinate measuring machine. The measured response characteristics for the proposed experimental design are presented in Table 2.

Table 2. Experiment details based on RSM-BBD and their measured responses.

Exp. No.	Dependent Variables				Output Responses		
	r-GO (wt%)	Traverse Speed (mm/min)	Waterjet Pressure (MPa)	Nozzle Height (mm)	Material Removal Rate (g/s)	Delamination Factor	Kerf Deviation (mm)
1	0	400	250	3	3.089	2.141	1.857
2	2	400	250	3	3.338	2.132	1.937
3	0	600	250	3	3.105	1.822	1.825
4	2	600	250	3	3.115	2.317	1.851
5	1	500	200	2	3.233	2.09	2.148
6	1	500	300	2	2.993	2.048	2.136
7	1	500	200	4	3.323	2.157	2.196
8	1	500	300	4	3.136	2.248	1.897
9	0	500	250	2	2.994	1.902	1.857
10	2	500	250	2	2.945	2.006	2.201
11	0	500	250	4	2.937	1.924	2.057

Table 2. *Cont.*

Exp. No.	r-GO (wt%)	Dependent Variables			Output Responses		
		Traverse Speed (mm/min)	Waterjet Pressure (MPa)	Nozzle Height (mm)	Material Removal Rate (g/s)	Delamination Factor	Kerf Deviation (mm)
12	2	500	250	4	3.173	2.301	1.802
13	1	400	200	3	3.389	2.196	2.094
14	1	600	200	3	3.457	2.217	2.019
15	1	400	300	3	3.329	2.322	1.937
16	1	600	300	3	3.081	2.153	1.889
17	0	500	200	3	3.329	1.9	1.977
18	2	500	200	3	3.396	2.175	2.245
19	0	500	300	3	3.058	1.942	2.057
20	2	500	300	3	3.233	2.196	1.884
21	1	400	250	2	3.009	2.193	1.977
22	1	600	250	2	3.073	2.006	1.958
23	1	400	250	4	3.245	2.259	1.912
24	1	600	250	4	2.977	2.28	1.826
25	1	500	250	3	3.045	2.18	2.126
26	1	500	250	3	3.057	2.19	2.117
27	1	500	250	3	3.059	2.213	2.116
28	1	500	250	3	3.073	2.204	2.112
29	1	500	250	3	3.079	2.188	2.122

4. Results and Discussion

In order to assess the effectiveness of the experimental approach, it was necessary to undertake statistical analysis on the conducted experiments and the resulting response variables. The study used a multi-parametric analysis of variance (ANOVA) to examine several statistical measures, including the coefficient of determination, sum of squares, lack of fit, individual, interaction, quadratic effects, and F-statistics. This analysis was conducted on chosen response features, namely *MRR*, *FD*, and *KD*, of the test samples processed using the AWJ cutting process. The investigation was carried out in three distinct phases. Initially, ANOVA was used to assess the statistical significance and the impact of selected independent parameters on the performance and quality characteristics of cut specimens. The subsequent phase included the formulation of second-order polynomial equations for each response feature, with the aim of establishing the correlation between the selected dependent variables and the features of the response. During the third step, the metaheuristic algorithms were used to identify the most optimal parametric combinations.

4.1. Statistical Analysis of Developed Polynomial Models

Multi-parametric ANOVA is used to conduct comprehensive investigations on the statistical implications of response characteristics acquired from experimental data. Tables 3–5 provide the findings of the ANOVA for selected output responses, including *MRR*, *FD*, and *KD*. With a 95% level of confidence, the AWJ cutting experiments were carried out, and Design Expert™ 13 software was used to perform the statistical analysis. The development of quadratic polynomial models for subsequent studies followed an analysis of statistical indicators such individual and interaction effects, coefficient of determination, lack of fit, and sum of squares. The stated AWJ cutting variables have a considerable influence on the response features, according to the statistical results from ANOVA. The lack-of-fit values were also found to be statistically significant within the chosen range of processing parameters, indicating the significance of the experiments that were carried out. In addition, the backward elimination technique was used to exclude the insignificant parametric terms with probabilities greater than 0.05 from the ANOVA in order to develop polynomial models. Multiple-regression coefficients (R^2) of 0.9955, 0.9954, and 0.9992 for *MRR*, *FD*, and *KD*, respectively, indicate the closeness of the derived models to the actual data.

Equations (11)–(13) represent the obtained polynomial regression models following the elimination of insignificant parameter combinations. Residual plots were used in addition to ANOVA to statistically confirm the results of the accomplished AWJ cutting experimental trials. Figure 3a–c provide a summary of the statistical analysis conducted for each response characteristic. Based on the summary reports, it has been observed that the distribution of data points along the center line provides evidence of the statistical significance of the developed models, as demonstrated by the normal probability plots. Additionally, the distributional frequency of data, as depicted by the histogram, shows that the measured responses are well constructed at a 95% confidence level. These findings indicate that the measured experimental data can be effectively utilized for further investigations.

$$
\begin{aligned}
MRR(g/s) = {} & 6.433 - 0.028 \times A - 0.0014 \times B - 0.0302 \times C + 0.721 \times D \\
& - 0.0006 \times AB + 0.0005 \times AC + 0.0712 \times AD - 0.00002 \times BC - 0.0008 \times BD \\
& + 0.0178 \times A^2 + 7.97 \times 10^{-6} \times B^2 + 0.00007 \times C^2 - 0.067 \times D^2
\end{aligned} \tag{11}
$$

$$
\begin{aligned}
FD = {} & 2.877 - 0.434 \times A - 0.004 \times B + 0.006 \times C - 0.161 \times D + 0.001 \times AB \\
& + 0.068 \times AD - 0.000009 \times BC + 0.0005 \times BD + 0.0007 \times CD - 0.125 \times A^2 \\
& + 3.529 \times 10^{-6} \times B^2 - 5.583 \times 10^{-6} \times C^2 - 0.0427 \times D^2
\end{aligned} \tag{12}
$$

$$
\begin{aligned}
KD\ (mm) = {} & -3.345 + 1.285 \times A + 0.015 \times B + 0.00041 \times C + 0.8086 \times D \\
& - 0.0001 \times AB - 0.002 \times AC - 0.149 \times AD + 1.35 \times 10^{-6} \times BC - 0.0002 \times BD \\
& - 0.001 \times CD - 0.096 \times A^2 - 1.548 \times 10^{-5} \times B^2 + 7.91 \times 10^{-6} \times C^2 - 0.044 \times D^2
\end{aligned} \tag{13}
$$

Table 3. Statistical analysis of *MRR*.

Sources	SS	DF	MS	F	Prob > F	
Model	0.6130	14	0.04379	224.815	<0.0001	Significant
A-*r-GO*	0.03944	1	0.03944	202.510	<0.0001	
B-*TS*	0.02910	1	0.02910	149.432	<0.0001	
C-*WP*	0.14018	1	0.14018	719.696	<0.0001	
D-*NH*	0.02466	1	0.02466	126.609	<0.0001	
AB	0.01428	1	0.01428	73.313	<0.0001	
AC	0.00291	1	0.00291	14.970	0.0017	
AD	0.02030	1	0.02030	104.251	<0.0001	
BC	0.02496	1	0.02496	128.163	<0.0001	
BD	0.02755	1	0.02755	141.470	<0.0001	
A^2	0.00206	1	0.00206	10.580	0.0058	
B^2	0.04120	1	0.04120	211.532	<0.0001	
C^2	0.19514	1	0.19514	1001.864	<0.0001	
D^2	0.02862	1	0.02862	146.934	<0.0001	
Residual	0.00272	14	0.00019			
Lack of Fit	0.00199	10	0.00019	1.091	0.5085	Insignificant
Pure Error	0.00073	4	0.00018			
R^2	99.55%		Adj. R^2	99.11%		

Table 4. Statistical analysis of *FD*.

Sources	SS	DF	MS	F	Prob > F	
Model	0.51333	14	0.03666	223.756	<0.0001	Significant
A-*r-GO*	0.18650	1	0.18650	1138.112	<0.0001	
B-*TS*	0.01672	1	0.01672	102.065	<0.0001	
C-*WP*	0.00252	1	0.00252	15.396	0.0015	
D-*NH*	0.07114	1	0.07114	434.175	<0.0001	
AB	0.06350	1	0.06350	387.528	<0.0001	
AD	0.01863	1	0.01863	113.702	<0.0001	
BC	0.00902	1	0.00902	55.074	<0.0001	
BD	0.01081	1	0.01081	66.003	<0.0001	
CD	0.00442	1	0.00442	26.986	0.0001	
A^2	0.10087	1	0.10087	615.606	<0.0001	
B^2	0.00807	1	0.00807	49.301	<0.0001	
C^2	0.00126	1	0.00126	7.712	0.0148	
D^2	0.01183	1	0.01183	72.200	<0.0001	
Residual	0.00229	14	0.00016			
Lack of Fit	0.00159	10	0.00015	0.9035	0.5945	Insignificant
Pure Error	0.00070	4	0.000176			
R^2	99.54%		Adj. R^2	99.12%		

Table 5. Statistical analysis of *KD*.

Sources	SS	DF	MS	F	Prob > F	
Model	0.48251	14	0.03446	1343.006	<0.0001	Significant
A-*r-GO*	0.00700	1	0.00700	273.089	<0.0001	
B-*TS*	0.00997	1	0.00997	388.742	<0.0001	
C-*WP*	0.06438	1	0.06438	2508.923	<0.0001	
D-*NH*	0.02871	1	0.02871	1118.886	<0.0001	
AB	0.00072	1	0.00072	28.406	0.0001	
AC	0.04862	1	0.04862	1894.559	<0.0001	
AD	0.08970	1	0.08970	3495.301	<0.0001	
BC	0.00018	1	0.00018	7.101	0.0185	
BD	0.00112	1	0.00112	43.730	<0.0001	
CD	0.02059	1	0.02059	802.407	<0.0001	
A^2	0.06020	1	0.06020	2346.004	<0.0001	
B^2	0.15551	1	0.15551	6060.049	<0.0001	
C^2	0.00253	1	0.00253	98.923	<0.0001	
D^2	0.01268	1	0.01268	494.165	<0.0001	
Residual	0.00035	14	2.5×10^{-5}			
Lack of Fit	0.00024	10	2.4×10^{-5}	0.805	0.6457	Insignificant
Pure Error	0.00011	4	0.00002			
R^2	99.92%		Adj. R^2	99.85%		

4.2. Influence of AWJ Cutting Parameters on Response Characteristics

Increased *MRR* with reduced *FD* and *KD* are desirable during the mechanical-based AWJ cutting process to enhance cutting quality. An enhanced *MRR* is often sought by manufacturing industries to improve the production rate while also reducing manufacturing costs, and *FD* and *KD* are quality indices of processed end-use components that should be decreased. The refining of the delamination factor and the reduction in kerf deviation have considerably improved the precision of the cutting process, reducing inaccuracy during assembly and decreasing substrate material depletion. From the statistical investigation results, the considered AWJ cutting parameters and the addition of r-GO nano fillers to the fabrication of FILs has a significance influence on the cut quality characteristics.

Figure 4a–f provide valuable insights into the intricate relationship between the AWJ cutting parameters and the cut quality characteristics, where two variables are varied while the other two variables are kept unchanged. From the statistical investigation, it is found

that all the selected process parameters have a significant influence on *MRR* (Table 3). The influence of the addition of r-GO and the nozzle height on the *MRR* is indicated in Figure 4a. From the response surface plot, the maximized *MRR* was attained at an augmented nozzle height (4 mm) and r-GO addition (2 wt%). An increase in nozzle height causes depth craters by increasing the momentum of hard abrasive particles that contact the substrate. In turn, this increases substrate surface erosion, allowing for the recovery of increased *MRR* [19]. The impact of traverse speed and the waterjet pressure on the *MRR* is indicated in Figure 4b. The surface plot indicates that the *MRR* was increased linearly by increasing the traverse speed as well as the waterjet pressure. However, the maximized *MRR* was attained at higher traverse speed (600 mm/min) or higher waterjet pressure (200 MPa). This may be attributed to the hard erosion of abrasive particles at higher jet pressure, along with maximized cutting speed, which leads to an improved removal of substrate [14].
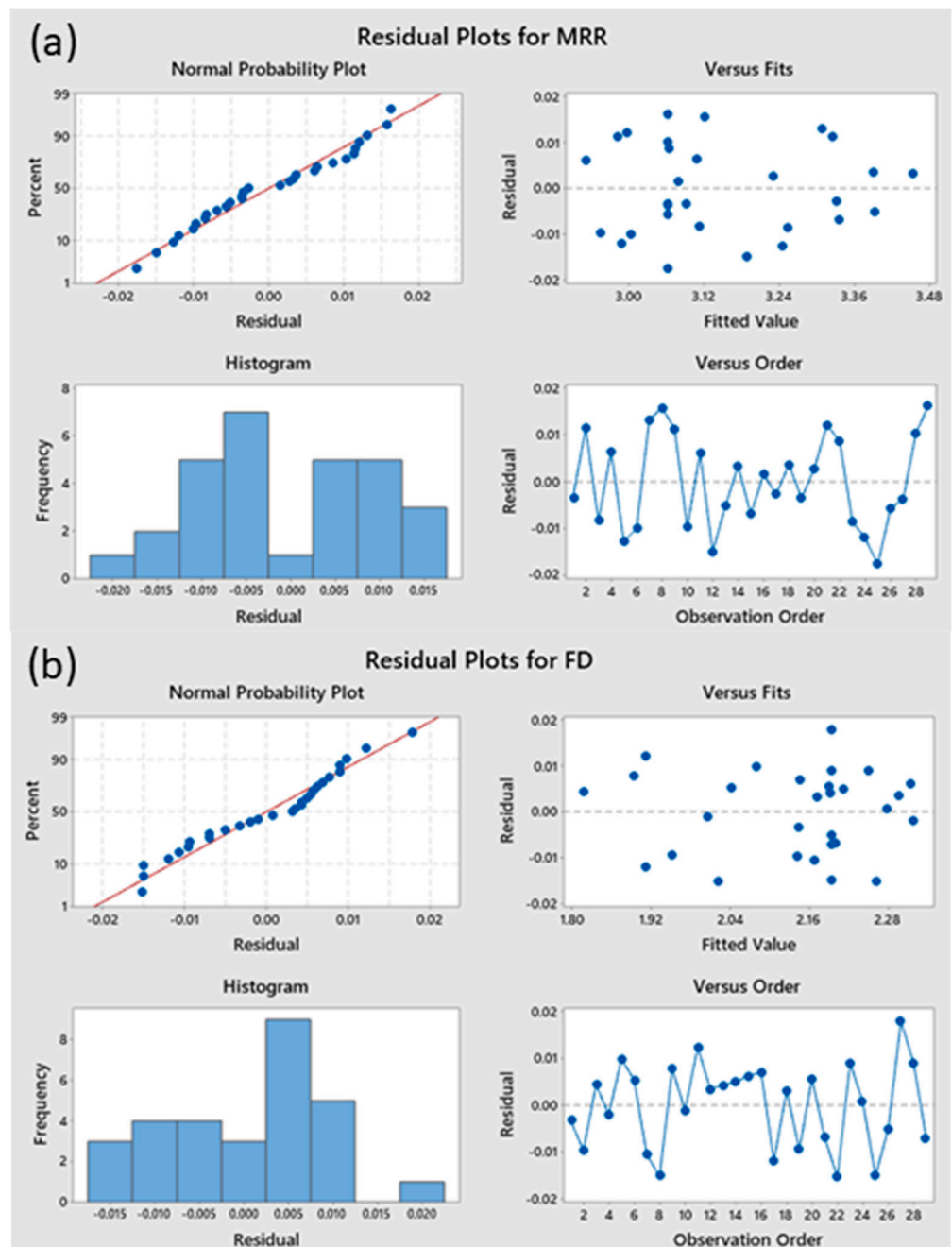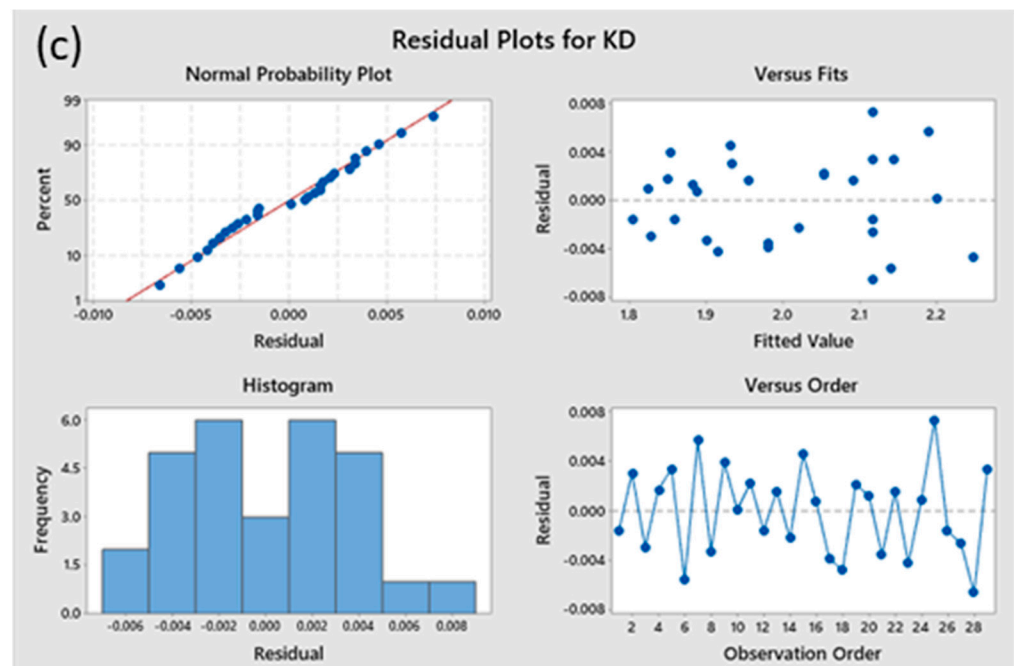

Figure 3. *Cont.*

Figure 3. Statistical validation of proposed models: (**a**) *MRR*, (**b**) *FD*, and (**c**) *KD*.

Figure 4c,d shows the influence of AWJ parameters on the delamination factor of the machined FILs at different cutting conditions. From the plots, it is perceived that the *FD* was increased with an increase in all the selected parameters, whereas the quantified *FD* was seen at lower waterjet pressure, nozzle height, and unreinforced FILs. This may be attributed to the complete fracture and debonding of plies in FILs due to higher energy levels associated with the pressurized waterjet, which leads to an augmented delamination [20]. Furthermore, it is noted that the waterjet bends at greater traverse speeds, which produces a curved cutting front that results in the highest normal force. As a result, the metal-composite interface sustains significant damage, which increases the factor of delamination [21].

The effects of AWJ cutting parameters on the kerf deviation are shown in response surface plots (Figure 4e,f). The kerf deviation is found linear increase with an increase in traverse speed and addition of r-GO fillers up to a certain level, and then decreasing, whereas it is found to linearly increase with an increase in nozzle height and waterjet pressure. A faster traverse speed during the AWJ cutting process permits abrasive particles to travel swiftly across the substrate, resulting in an incorrect cutting kerf and decreased quality characteristics. Therefore, keeping a consistent traverse speed is critical to achieve a lower kerf variation [22]. Moreover, the peak velocity of the waterjet expands (the jet diverges) when it leaves the mixing chamber at a greater nozzle height. When the jet swerves, kinetic energy is lost during penetration of the substrate surface, and it may not have enough force on its visible surface to cut effectively. This effect causes kerf deviation to rise as nozzle height increases [23].

4.3. Optimization of AWJ Cutting Process

The objective of this study is to address an optimization problem that involves the simultaneous optimization of multiple objectives; specifically, to maximize the *MRR* while minimizing the *FD* and *KD*. To achieve this, the decision variables associated with the AWJ cutting process, including traverse speed, waterjet pressure, and nozzle height, along with the impact of incorporating reduced graphene oxide (r-GO) in the composite laminates, were considered for optimization. In general, a process parameter set for one objective function cannot be used for any other objective functions. Since the objective functions chosen for this study conflict with each other, the optimization process is difficult. Usually,

there are two ways to solve such complicated optimization problems. The first is to turn multiple objectives into a single objective by giving each objective a weight or a utility function. The second is to find non-dominated Pareto optimum settings for the decision variables [24]. This study utilizes non-dominated solutions for each response characteristic to obtain the optimal processing parameters.
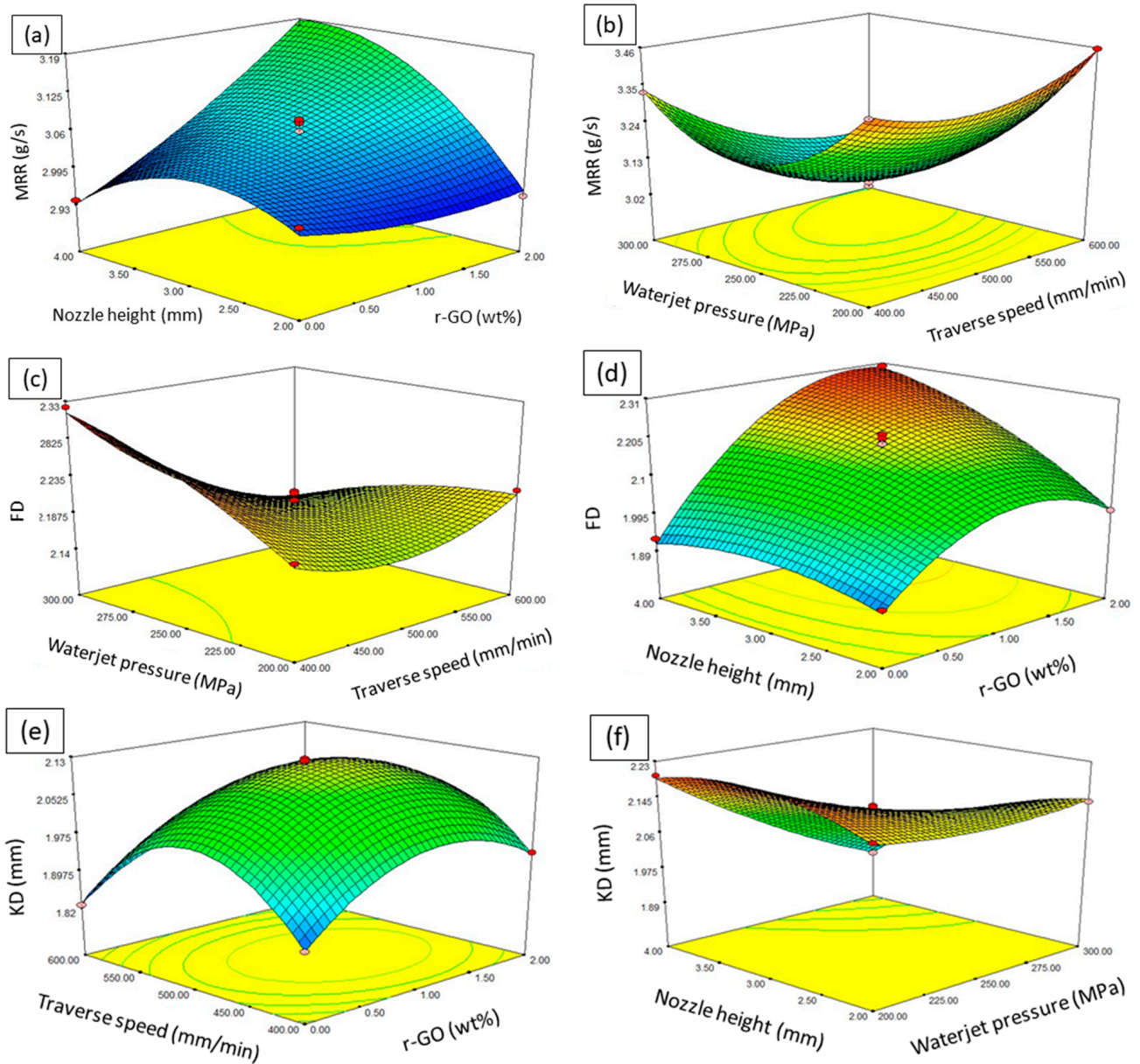

Figure 4. Effect of AWJ cutting parameters and wt% of r-GO on the response characteristics: (**a**,**b**) *MRR*, (**c**,**d**) *FD*, and (**e**,**f**) *KD*.

The objective functions for the present optimization work are formulated using the second-order polynomial equations obtained through the statistical analysis (Equations (11)–(13)) and the boundary conditions of the selected processing parameters (Table 1). For the multi-objective optimization, a highly versatile metaheuristic-based moth–flame optimization (MFO) algorithm was considered to simultaneously improve the *MRR* and minimize the *FD* and *KD* of AWJ-processed FILs. In order to assess the performance characteristics of the proposed MFO algorithm, several established meta-heuristic algorithms were taken into consideration. These algorithms include the genetic algorithm (GA), particle swarm optimization (PSO) algorithm, dragonfly algorithm (DFO),

and grey-wolf optimization algorithm (GWO). By comparing various performance features, such as convergence plot, diversity, spacing, and hypervolume values, a comprehensive evaluation of the MFO algorithm can be achieved.

The proposed optimization algorithms were executed in a MATLAB 2022b™ environment with a population size and number of iterations of 30 and 100, respectively, for each algorithm. The parameters used for executing different optimization algorithms to obtain non-dominated Pareto optimal solutions are shown in Table 6. Each optimization algorithm was executed thirty-six times to obtain the number of Pareto optimal solutions. For each execution, an optimal combination of process parameters and their corresponding response values were determined and considered as the best solution for that execution. Similarly, each algorithm yielded thirty-six sets of optimal parameters for each response characteristic, which were considered for further investigations. Figure 5a–c depict a sample convergence plot derived for each response characteristic using various algorithms. Among the obtained thirty-six non-dominated Pareto optimal solutions, Deng's similarity-based analytical hierarchy approach [25] was adopted for each algorithm to obtain the optimal solution based on the overall performance index. The optimal AWJ cutting parameters and their corresponding response characteristics, such as *MRR*, *FD*, and *KD*, achieved through Deng's approach, are listed in Table 7.

Table 6. Parameters and their values used in GA, PSO, MFO, DFO, and GWO.

Algorithm	Parameters	Value/Range of Parameters
GA	Method of Selection for Reproduction	Roulette Wheel Selection Method
	Cross over probability	0.5
	Cross over operator	Single Point Cross Over Technique
	Mutation probability	0.04
	Mutation operator	Right-side swapping
	Replacement strategy	100% replacement Strategy
PSO	Learning factors (*C1* and *C2*)	2 and 2
	Inertia weight (ω)	0.9
MFO	Position of moth close to the flame (*t*)	-1 to -2
	Update mechanism	Logarithmic spiral
DFO	Inertia weight (*IW*)	0.2
	Separation weight	$sw = 0.1 - \frac{0.1 * itr}{nitr}$
	Alignment weight	$aw = 0.1 - \frac{0.1 * itr}{nitr}$
	Cohesion weight	$aw = 0.1 - \frac{0.1 * itr}{nitr}$
	Food factor	$ff = 2 * rand$
	Enemy factor	$ef = 0.1 - \frac{0.1 * itr}{nitr}$
GWO	Scale Factor (*SF*)	2

Table 7. Optimal AWJ cutting parameter achieved through different algorithms.

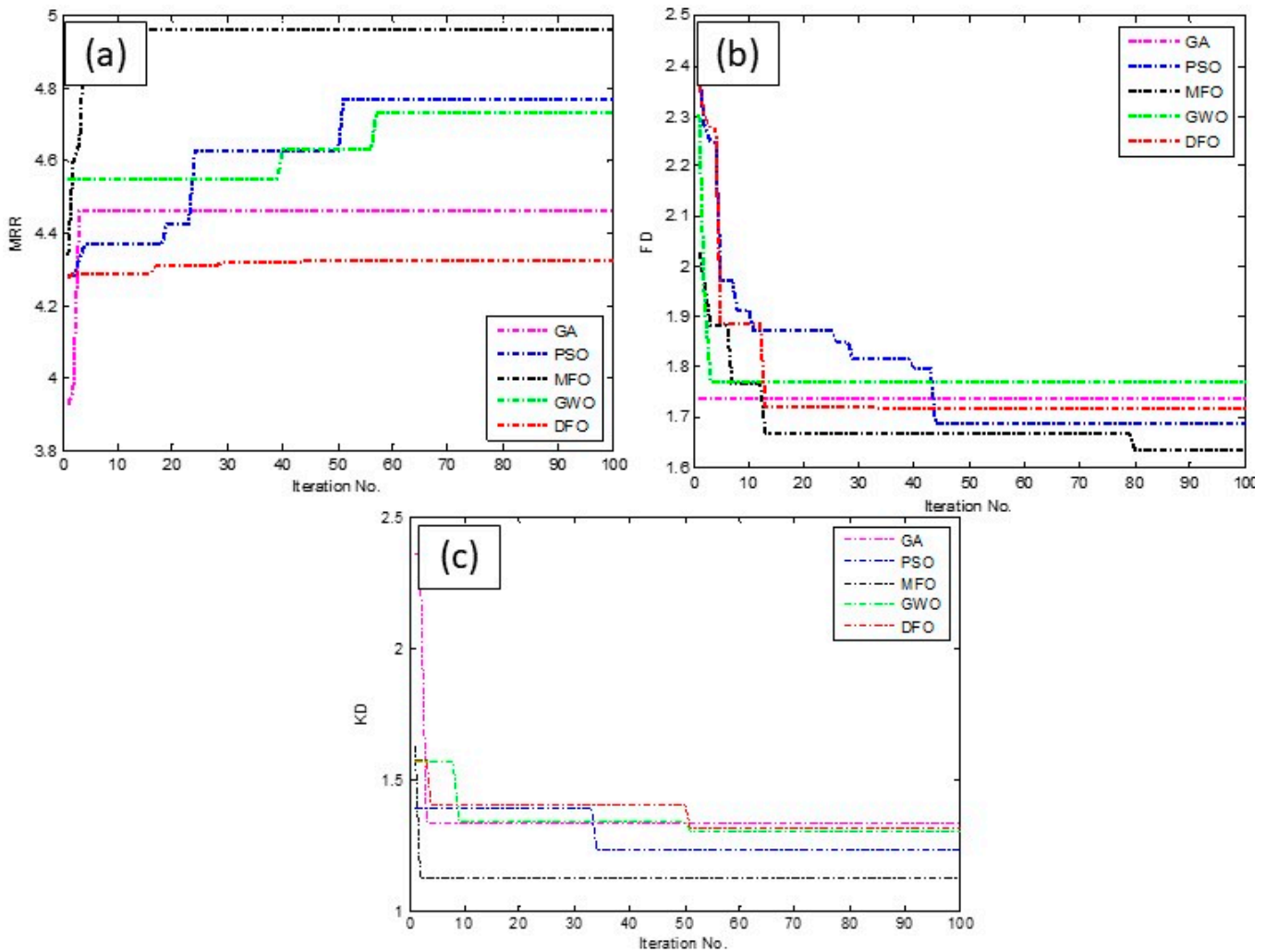| Algorithms	*r-GO*	*TS*	*JP*	*NH*	*MRR*	*FD*	*KD*
GA	0.004	561.74	277.89	2.02	2.963	1.945	1.972
PSO	0.038	592.68	261.92	2.07	3.045	1.951	1.893
MFO	0.000	600.00	253.36	2.00	3.096	1.928	1.833
GWO	0.026	595.67	255.66	2.04	3.074	1.947	1.865
DFO	0.000	600.00	246.80	2.00	3.127	1.935	1.819

Figure 5. Convergence plots for: (**a**) *MRR*, (**b**) *FD*, and (**c**) *KD* obtained through different metaheuristic algorithms.

4.4. Comparison of MFOA Performance with State-of-the-Art Metaheuristic Algorithms

In this section, the effectiveness of MFO is compared to that of other metaheuristic strategies such as GA, PSO, GWO, and DFO. The results of this comparison analysis show how MFO is more efficient than other algorithms in AWJ cutting applications. From the convergence plots shown in Figure 5a–c, MFO is found to outperform the similar algorithms in terms of the convergence with minimal iterations. MFO converges quickly (i.e., the number of iterations for MRR is 5, that for FD is 12, and that for KD is 3) to obtain the optimal solutions; hence, the execution time of MFO can be significantly minimized for such complex optimization problems relative to the compared metaheuristics.

4.4.1. Diversity Values

Diversity values are used to quantify the difference or similarity of the solutions produced by each algorithm throughout the optimization or decision-making process. Diversity values not only help to determine which strategy is best for a particular optimization problem, but also provide insight into the flexibility and resilience of certain algorithms in situations when complicated decisions must be made [26]. The diversity

values between the two successive optimal solutions were calculated based on the following mathematical relation:

$$D = \sqrt{\sum_{j=1}^{k} \left(f_j^{\max} - f_j^{\min} \right)^2} \tag{14}$$

The diversity values for selected algorithms are depicted in Table 8. The diversity values for all the algorithms exhibited a high degree of similarity. The statistical analysis, including the Anderson–Darling normality test, normal probability analysis, and analysis of variance, was conducted on the diversity values obtained in order to assess the performance of the algorithms. Based on the data presented in Table 9, it can be observed that the statistical indicators of MFO algorithms demonstrate superior performance compared to other optimization algorithms. Traditionally, diversity values have been evaluated using a higher-the-better approach. The *p*-value for the MFO algorithm is determined to be lower (0.006) in comparison to that of other metaheuristic algorithms. Therefore, the MFO algorithm demonstrates superior performance in optimizing the AWJ cutting parameters. The significance of the proposed algorithms is confirmed by the normal probability plots depicted in Figure 6a–e at a 95% confidence interval. Furthermore, the statistical significance of the proposed algorithms was confirmed by Friedman's ANOVA, as depicted in Figure 7, with a probability of less than 0.05.
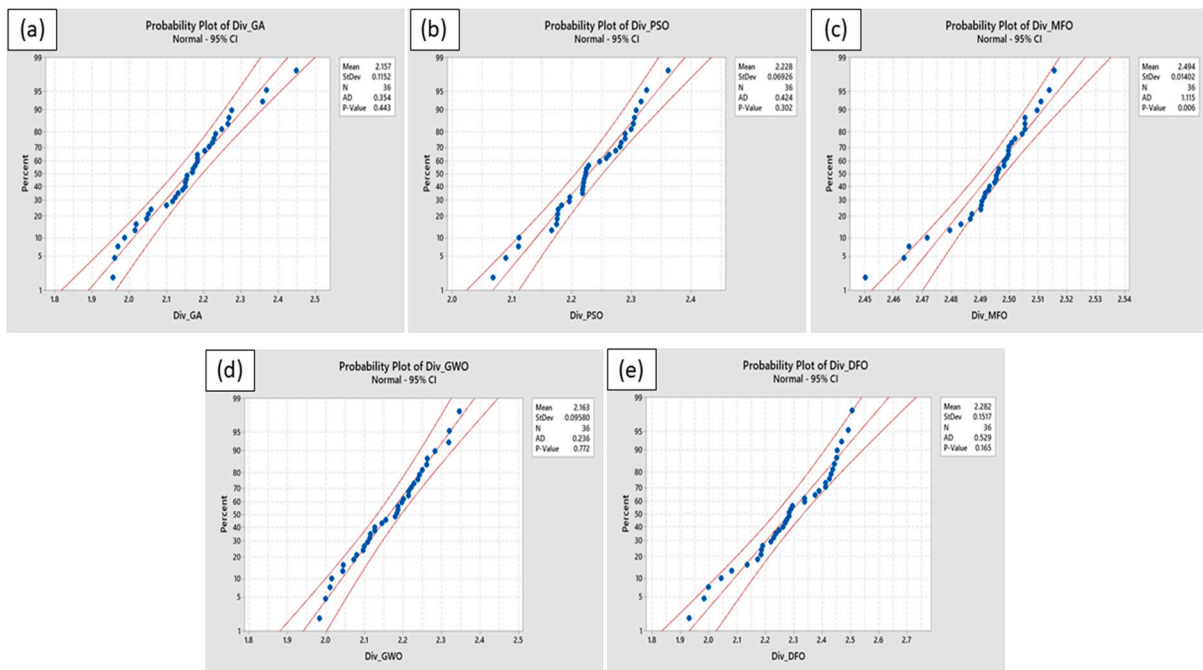

Figure 6. Normal probability plots for diversity values of: (**a**) GA, (**b**) PSO, (**c**) MFO, (**d**) GWO, and (**e**) DFO.

Figure 7. Friedman's statistical results for diversity values obtained through different algorithms.

Table 8. Diversity values for different algorithms.

R. No.	GA	PSO	MFO	GWO	DFO
1	2.168649	2.304893	2.499654	2.043835	2.375572
2	2.213475	2.218671	2.479363	2.228079	2.171757
3	1.969053	2.217624	2.495559	2.009252	2.135089
4	2.181977	2.228235	2.463419	2.014581	2.228036
5	1.955133	2.289423	2.495492	2.186953	1.928915
6	2.01437	2.262722	2.450018	1.998452	2.443005
7	2.227546	2.289307	2.49616	2.197105	2.282027
8	2.358251	2.08906	2.499123	2.237759	2.282308
9	2.201808	2.325128	2.471608	2.18695	2.29433
10	2.170561	2.223838	2.493166	2.262642	2.189975
11	2.368679	2.361817	2.502011	2.214497	2.388704
12	2.149618	2.217916	2.465304	2.126008	1.981838
13	2.267597	2.316509	2.48331	2.125932	2.184926
14	2.100045	2.280508	2.504573	2.155223	2.269794
15	2.231728	2.303261	2.492761	2.319721	2.492793
16	2.150087	2.06787	2.490507	2.260906	2.452572
17	2.154984	2.2825	2.491626	2.28224	2.437811
18	2.1229	2.257634	2.49007	2.072323	2.236772
19	2.248569	2.176258	2.487019	2.21459	2.217735
20	1.959028	2.182378	2.496555	2.249677	2.430681
21	2.176041	2.219705	2.513995	2.099185	2.336751
22	2.182276	2.24678	2.50539	2.04243	2.468178
23	2.152185	2.299786	2.494864	2.242218	2.505339
24	2.222158	2.174597	2.505402	2.221646	2.289126
25	2.058078	2.222779	2.515658	2.318232	2.426425
26	2.14218	2.195657	2.499704	2.079501	2.412103
27	2.018371	2.308123	2.499831	2.113446	2.262402
28	2.275256	2.166078	2.490278	2.17957	1.997895
29	2.129946	2.110984	2.509637	2.114911	2.247057
30	2.182925	2.273363	2.49827	1.982684	2.411676
31	2.045438	2.17486	2.5008	2.184017	2.274243
32	2.049843	2.220535	2.511027	2.096799	2.042195
33	2.265088	2.224345	2.491387	2.20141	2.337978
34	2.115209	2.110337	2.498101	2.144963	2.450462
35	2.449285	2.177214	2.486478	2.107356	2.183684
36	1.986994	2.196914	2.505473	2.345533	2.080497

Table 9. Statistical analysis results for diversity values (the higher the better).

	Mean	Median	StDev	*p*-Value	A-Squared
GA	2.1574	2.1618	0.1152	0.443	0.35
PSO	2.2283	2.2233	0.0693	0.302	0.42
MFO	2.4937	2.4959	0.014	0.006	1.11
GWO	2.1628	2.1818	0.0958	0.772	0.24
DFO	2.282	2.2822	0.1517	0.165	0.53

4.4.2. Spacing Values

The evaluation of the algorithms' performance via the adjustment of spacing values is an essential process in enhancing their efficiency and efficacy. This research assessed five algorithms, and the findings provided insights into the individual strengths and limitations of each algorithm. The spacing values, which denote the distance between data points or items inside the algorithmic process, were significant in influencing the resulting performances. The spacing values can be calculated by the following relation [27]:

$$Spacing = \sqrt{\frac{1}{nr-1}\sum_{i=1}^{nr}\left(\overline{S}-S_i\right)^2} \qquad (15)$$

where S_i denotes the minimum value of the sum of the absolute difference between the ith run and all other runs, $\overline{S}$ indicates the mean value of S_i, and nr indicates the number of runs. S_i and $\overline{S}$ can be calculated as follows:

$$S_i = \min_{i=1,2\ldots nr} \left\{ \sum_{j=1}^{no} abs\left(O_{ij} - O_{kj} \right) \right\}_{k=i+1,\ldots nr} \tag{16}$$

$$\overline{S} = \frac{\sum_{i=1}^{nr} S_i}{nr} \tag{17}$$

Table 10 illustrates the spacing values for selected algorithms. It is observed that the spacing values for all the algorithms were close to each other. Hence, the statistical analysis, such as the Anderson–Darling normality test, normal probability analysis, and analysis of variance, was performed for the obtained spacing values to identify the performance of the algorithms. From Table 11, it is perceived that the statistical indicators of the MFO algorithms are found to be better than those of the other optimization algorithms. In general, lower spacing values are considered to be better. The *p*-value of MFO is found to be less (0.077) that that of the compared similar metaheuristics. Hence, the MFO algorithms outperform when optimizing the AWJ cutting parameters. Moreover, the normal probability plots, as shown in Figure 8a–e, at a 95% confidence interval, confirm the significance of the proposed algorithms. In addition to these indicators, Friedman's ANOVA, as shown in Figure 9, proved the statistical significance of the proposed algorithms with a probability of less than 0.05.
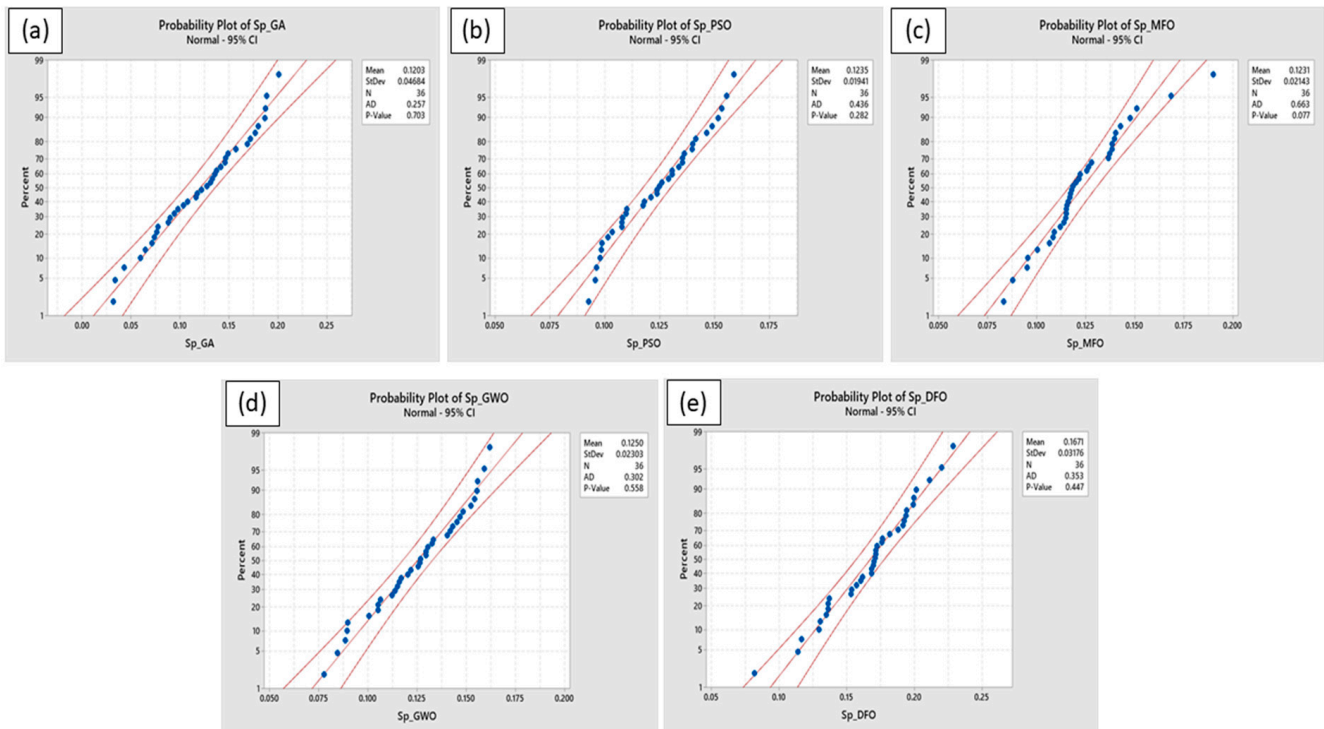

Figure 8. Normal probability plots for spacing values of: (**a**) GA, (**b**) PSO, (**c**) MFO, (**d**) GWO, and (**e**) DFO.

Friedman's ANOVA Table

```
Source      SS       df      MS      Chi-sq    Prob>Chi-sq
--------------------------------------------------------------
Columns    87.722     4    21.9306    35.09    4.45408e-07
Error     272.278    140    1.9448
Total      360       179
```

Figure 9. Friedman's statistical results for spacing values obtained through different algorithms.

Table 10. Spacing values for different algorithms.

R. No.	GA	PSO	MFO	GWO	DFO
1	0.171861	0.12602	0.095347	0.140296	0.22027
2	0.077513	0.148809	0.13961	0.148331	0.175924
3	0.179912	0.129001	0.168505	0.100561	0.153444
4	0.137394	0.11805	0.140185	0.141723	0.199079
5	0.059374	0.153299	0.095116	0.129341	0.129182
6	0.089924	0.133724	0.138516	0.155851	0.187791
7	0.031828	0.123791	0.119912	0.115053	0.160384
8	0.121846	0.107809	0.115156	0.088389	0.2012
9	0.168761	0.130516	0.087649	0.116846	0.19233
10	0.103402	0.107863	0.121393	0.115857	0.134854
11	0.127415	0.139783	0.138381	0.077522	0.081749
12	0.075933	0.109626	0.126515	0.133277	0.211131
13	0.146091	0.092408	0.115436	0.146942	0.171441
14	0.149202	0.123644	0.125337	0.161928	0.161768
15	0.177037	0.098677	0.136648	0.159245	0.168211
16	0.117693	0.135384	0.108884	0.106243	0.181798
17	0.131298	0.097819	0.114563	0.120059	0.194169
18	0.073594	0.146526	0.128028	0.145166	0.228594
19	0.156817	0.15169	0.147622	0.121731	0.16827
20	0.132661	0.140057	0.114989	0.132636	0.17157
21	0.087826	0.141518	0.100301	0.129533	0.153153
22	0.09749	0.098401	0.08295	0.112057	0.176316
23	0.033361	0.155446	0.137077	0.089675	0.172437
24	0.071403	0.130527	0.115946	0.084484	0.1369
25	0.094119	0.136201	0.142586	0.089393	0.191336
26	0.043007	0.135437	0.106377	0.12631	0.11356
27	0.116329	0.124705	0.116774	0.14302	0.116459
28	0.135279	0.117342	0.118517	0.155435	0.19377
29	0.1078	0.096062	0.111802	0.154188	0.130144
30	0.187168	0.109787	0.122027	0.113683	0.171007
31	0.146462	0.121002	0.15111	0.126761	0.136029
32	0.188334	0.107605	0.190077	0.105073	0.169524
33	0.20072	0.158927	0.117647	0.130279	0.199426
34	0.064219	0.103374	0.117306	0.125585	0.13606
35	0.186487	0.095541	0.108307	0.152431	0.15704
36	0.141557	0.101333	0.113652	0.105075	0.169872

Table 11. Statistical analysis results for spacing values (the lower the better).

	Mean	Median	StDev	*p*-Value	A-Squared
GA	0.12031	0.12463	0.04684	0.703	0.26
PSO	0.12355	0.12425	0.01941	0.282	0.44
MFO	0.12306	0.11805	0.02143	0.077	0.66
GWO	0.125	0.12654	0.02303	0.558	0.3
DFO	0.16712	0.17044	0.03176	0.447	0.35

4.4.3. Hypervolume Values

The hypervolume metric has significant importance within the field of optimization techniques, especially in the context of multi-objective optimization. It measures how well an algorithm can explore and cover the Pareto front, which is a collection of non-dominated solutions that reflect the best trade-offs between many competing goals. It is a key indicator of the quality of a solution. One may evaluate the coverage, variety, and effectiveness of an algorithm's solutions by computing the hypervolume. A more thorough examination of the goal space is indicated by higher hypervolume values, which also indicate better solution quality performance [28]. The mathematical expression for calculating the hypervolume can be defined as follows:

$$HV(PF) = \Lambda \left(\bigcup_{s \in PF} \left\{ S' : S \prec S' \prec S^{nadir} \right\} \right) \tag{18}$$

where *PF* is defined as the Pareto front, the point of approximation of *PF* can be expressed as *S*, the generalization of a volume is defined by Λ, and the domination relation may be defined by $\prec$. Table 12 presents the hypervolume values corresponding to the chosen algorithms. The hypervolume values for all the algorithms exhibited a high degree of similarity. The statistical analysis included the Anderson–Darling normality test, normal probability analysis, and analysis of variance. These tests were conducted on the obtained hypervolume values in order to assess the performance of the algorithms. Based on the data presented in Table 13, it can be observed that the statistical indicators of GA and DFO algorithms demonstrate superior performance compared to other optimization algorithms. Traditionally, the higher-the-better approach has been favored when evaluating hypervolume values. The *p*-values for GA and DFO were determined to be lower (0.022 and 0.024, respectively) when compared to those of other metaheuristics of a similar nature. Therefore, when evaluating the performance metric as the hypervolume, the GA and DFO algorithms were surpassed. The significance of the proposed algorithms was confirmed by the normal probability plots, as depicted in Figure 10a–e, at a 95% confidence interval. Furthermore, the statistical significance of the proposed algorithms was confirmed by Friedman's ANOVA, as depicted in Figure 11, with a probability of less than 0.05.
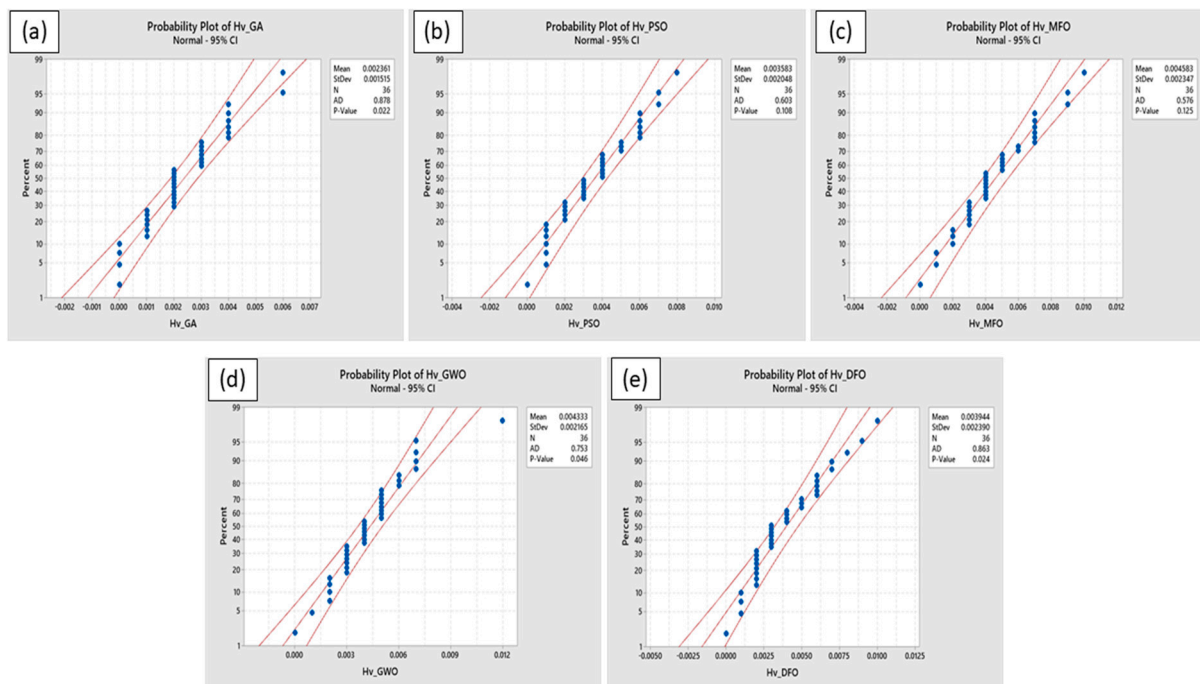

Figure 10. Normal probability plots for hypervolume values of: (**a**) GA, (**b**) PSO, (**c**) MFO, (**d**) GWO, and (**e**) DFO.

Table 12. Hypervolume values for different algorithms.

R. No.	GA	PSO	MFO	GWO	DFO
1	0.002	0.007	0.003	0.012	0.004
2	0.001	0.006	0.003	0.004	0.003
3	0.001	0.004	0.003	0.005	0.002
4	0.004	0.008	0.004	0.002	0.006
5	0.003	0.003	0.005	0.002	0.006
6	0.002	0.001	0.002	0.004	0.004
7	0.003	0.005	0.007	0.006	0.005
8	0.002	0.003	0.004	0.005	0.006
9	0.001	0.001	0.006	0.007	0.001
10	0.002	0.001	0.004	0.005	0.001
11	0.003	0.002	0.003	0.003	0.008
12	0.004	0.001	0.007	0	0.002
13	0.004	0.002	0.006	0.003	0.002
14	0.003	0.005	0.007	0.002	0
15	0.003	0.003	0.002	0.003	0.005
16	0.002	0.004	0.004	0.005	0.003
17	0	0.002	0.003	0.005	0.009
18	0.004	0.006	0.002	0.003	0.003
19	0.004	0.006	0.004	0.006	0.002
20	0.003	0.006	0.005	0.003	0.003
21	0.002	0.003	0.005	0.007	0.005
22	0.002	0.005	0.009	0.003	0.007
23	0.001	0.004	0.004	0.004	0.002
24	0.001	0.003	0.007	0.007	0.003
25	0.002	0.007	0.004	0.004	0.004
26	0.006	0.004	0.001	0.005	0.003
27	0.006	0.004	0.005	0.004	0.002
28	0	0.002	0.003	0.005	0.003
29	0.004	0.004	0.007	0.007	0.002
30	0.002	0.001	0.001	0.005	0.006
31	0.003	0.003	0.007	0.004	0.007
32	0.001	0	0	0.004	0.006
33	0.002	0.004	0.01	0.003	0.01
34	0	0.001	0.005	0.001	0.004
35	0.002	0.006	0.004	0.006	0.001
36	0	0.002	0.009	0.002	0.002

Table 13. Statistical analysis results for hypervolume values (the higher the better).

	Mean	Median	StDev	*p*-Value	A-Squared
GA	0.002361	0.002	0.001515	0.022	0.88
PSO	0.003583	0.0035	0.002048	0.108	0.6
MFO	0.004583	0.004	0.002347	0.125	0.58
GWO	0.004333	0.004	0.002165	0.046	0.75
DFO	0.003944	0.003	0.00239	0.024	0.86

```
                    Friedman's ANOVA Table

Source      SS        df      MS       Chi-sq    Prob>Chi-sq
-----------------------------------------------------------
Columns     44.431     4      11.1076   19.21      0.0007
Error       288.569  140       2.0612
Total       333      179
```

Figure 11. Friedman's statistical results for hypervolume values obtained through different algorithms.

The mean rank values of the optimization algorithms were assessed based on the performance indices, such as diversity, spacing, and hypervolume values, by conducting Friedman's statistical analysis [29]. To summarize the performance of distinct metaheuristics, the mean rank values were determined. The table displays the mean rank values for selected algorithms, and the MFO algorithm was found to provide higher performance index values, such as 4.9444 for diversity and 2.5833 for spacing, whereas GWO exhibits an improved hypervolume value of 3.5. When comparing the overall performance index, it can be inferred that the MFO algorithm exhibits superior performance in comparison to GA, PSO, GWO, and DFO while optimizing the AWJ cutting process based on the selected matrices, except for the hypervolume. Among the optimized parameters and their corresponding response characteristics obtained through different optimization algorithms, as shown in Table 14, the MFO algorithm's optimal values were considered as the best set of parameters to improve the cut quality and performance features of the AWJ cutting process. The corresponding optimal parameters were unreinforced laminate (i.e., 0 wt% r-GO), traverse speed of 600 mm/min, jet pressure of 253.36 MPa, and nozzle height of 2 mm, for improved response features, namely the corresponding *MRR*, *FD*, and *KD* values are 3.096 g/s, 1.928, and 1.833 mm, respectively. The optimal parameters show that the inclusion of nano fillers does not provide any significance regarding the selected cutting responses, whereas the lower nozzle height with the combination of higher traverse speed and medium jet pressure may enhance the selected cutting characteristics within the range of selected parameters.

Table 14. Mean rank values of different algorithms in Friedman's statistical analysis.

Performance Indicators	GA	PSO	MFO	GWO	DFO
Diversity	2.0833	2.7500	**4.9444**	2.0278	3.1944
Spacing	2.6667	2.5833	**2.5833**	2.7778	4.3889
Hypervolume	2.1111	2.9167	3.4306	**3.5000**	3.0417

4.5. Confirmation Experiments

In order to evaluate the rationality of the proposed optimization approach, a series of confirmation experiments were conducted. These experiments aimed to validate the effectiveness and efficiency of the proposed approach. The confirmation experiments were conducted thrice using the optimal AWJ cutting parameters obtained through the MFO algorithm. The average values of these experiments are shown in Table 15. The presented table demonstrates a relatively strong correlation between the predicted and experimentally measured response values. The average error for *MRR* is found to be 1.94%, while the average errors for *FD* and *KD* are 2.75% and 3.33%, respectively. These results indicate a satisfactory level of accuracy in the prediction of the response values.

Table 15. Confirmation experimental results of AWJ cutting responses at optimal parameters obtained through the MFO algorithm.

Responses	Predicted	Experimental	Error %
MRR (g/s)	3.096	3.156	1.94
FD	1.928	1.981	2.75
KD (mm)	1.833	1.772	3.33

5. Conclusions

In the present study, novel fiber intermetallic laminates were cut using AWJ by modifying the wt% of reduced graphene oxide in the laminates, traverse speed, jet pressure, and nozzle height. The influence of AWJ parameters on the cut quality characteristics was investigated, and multi-response optimization using five distinct metaheuristic algorithms, i.e., GA, PSO, MFO, GWO, and DFO, was accomplished. The performance features

of the algorithms were also investigated. The findings of this study are summarized as follows.

- The statistical analysis reveals that *JP* and *r-GO* addition have a significant influence on *MRR*, followed by *TS*, whereas *r-GO* addition and *NH* have a substantial impact on *FD*. In addition, it was observed that *KD* is significantly influenced by *WP* and *NH*.
- *MRR* is found to increase with an increase in *NH* and *JP* due to the increased momentum of hard abrasive particles that contact the substrate, which in turn increases substrate surface erosion, whereas it leads to augmented *FD* and *KD*, which deteriorate the cut quality. Therefore, it is necessary to maintain a consistent traverse speed, nozzle height, and jet pressure to achieve improved cut quality features.
- From the convergence plots, the MFO algorithm is found to converge more rapidly than similar metaheuristic algorithms due to its simplicity and the presence of minimal control parameters. Therefore, the space and time complexity can be significantly reduced by the MFO algorithm for optimizing such complex engineering problems.
- The optimal AWJ cutting parameters for improved quality features of FILs are unreinforced composite laminates (0 wt% of r-GO), 600 mm/min of *TS*, 253.36 MPa of *JP*, and 2 mm of *NH*. These parameter values were achieved using the moth–flame optimization algorithm.
- The suggested MFO algorithm also showed its efficacy in improving the quality and performance features of AWJ cutting by predicting appropriate parameter settings because the error variation between predicted and experimental measures was determined to be less than 3.5% for all the response characteristics of the cut specimens.
- The effectiveness of MFO was evaluated against GA, PSO, GWO, and DFO using the most widely used key metric indicators, including diversity, spacing, and hypervolume values. The comparative analysis results showed that the MFO algorithm produced lower spacing values and higher diversity and hypervolume values, which shows the efficiency of the algorithm.

The present work encompassed multi-response optimization of AWJ cutting parameters via different metaheuristic optimization algorithms with their standard control parameters. Future works may concentrate on tuning the algorithm parameters to improve their efficiency for better exploration and exploitation of similar optimization problems. Moreover, the effectiveness of the proposed algorithms may be improved by considering a range of workpiece materials, AWJ cutting parameters, and performance characteristics.

References

1. Costa, R.D.F.S.; Sales-Contini, R.C.M.; Silva, F.J.G.; Sebbe, N.; Jesus, A.M.P. A Critical Review on Fiber Metal Laminates (FML): From Manufacturing to Sustainable Processing. *Metals* **2023**, *13*, 638. [CrossRef]
2. Jamali, N.; Khosravi, H.; Rezvani, A.; Tohidlou, E. Mechanical properties of multiscale graphene oxide/basalt fiber/epoxy composites. *Fiber. Polym.* **2019**, *20*, 138–146. [CrossRef]

3. Saeimi Sadigh, M.A.; Marami, G. Investigating the effects of reduced graphene oxide additive on the tensile strength of adhesively bonded joints at different extension rates. *Mater. Des.* **2016**, *92*, 36–43. [CrossRef]

4. Emran, M.Y.; Miran, W.; Gomaa, H.; Ibrahim, I.; Belessiotis, G.V.; Abdelwahab, A.A.; Othman, M.B. Biowaste Materials for Advanced Biodegradable Packaging Technology. In *Handbook of Biodegradable Materials*; Springer International Publishing: Cham, Switzerland, 2022; pp. 1–37.

5. Smolnicki, M.; Lesiuk, G.; Duda, S.; de Jesus, A.M.P. A Review on Finite-Element Simulation of Fibre Metal Laminates. *Arch. Comput. Methods Eng.* **2023**, *30*, 749–763. [CrossRef]

6. Marques, F.; Silva, F.G.A.; Silva, T.E.F.; Rosa, P.A.R.; Marques, A.T.; de Jesus, A.M.P. Delamination of Fibre Metal Laminates Due to Drilling: Experimental Study and Fracture Mechanics-Based Modelling. *Metals* **2022**, *12*, 1262. [CrossRef]

7. Pai, A.; Kini, C.R.; Shenoy, B.S. Scope of Non-Conventional Machining Techniques for Fibre Metal Laminates: A Review. *Mater. Today* **2022**, *52*, 787–795. [CrossRef]

8. Siva Kumar, M.; Rajamani, D.; El-Sherbeeny, A.M.; Balasubramanian, E.; Karthik, K.; Hussein, H.M.A.; Astarita, A. Intelligent Modeling and Multi-Response Optimization of AWJC on Fiber Intermetallic Laminates through a Hybrid ANFIS-Salp Swarm Algorithm. *Materials* **2022**, *15*, 7216. [CrossRef]

9. Doğankaya, E.; Kahya, M.; Özgür Ünver, H. Abrasive Water Jet Machining of UHMWPE and Trade-off Optimization. *Mater. Manuf. Process.* **2020**, *35*, 1339–1351. [CrossRef]

10. Balamurugan, K.; Uthayakumar, M.; Sankar, S.; Hareesh, U.S.; Warrier, K.G.K. Predicting Correlations in Abrasive Waterjet Cutting Parameters of Lanthanum Phosphate/Yttria Composite by Response Surface Methodology. *Measurement* **2019**, *131*, 309–318. [CrossRef]

11. Kalirasu, S.; Rajini, N.; Winowlin Jappes, J.T.; Uthayakumar, M.; Rajesh, S. Mechanical and Machining Performance of Glass and Coconut Sheath Fibre Polyester Composites Using AWJM. *J. Reinf. Plast. Compos.* **2015**, *34*, 564–580. [CrossRef]

12. Alberdi, A.; Artaza, T.; Suárez, A.; Rivero, A.; Girot, F. An Experimental Study on Abrasive Waterjet Cutting of CFRP/Ti6Al4V Stacks for Drilling Operations. *Int. J. Adv. Manuf. Technol.* **2016**, *86*, 691–704. [CrossRef]

13. Hutyrová, Z.; Ščučka, J.; Hloch, S.; Hlaváček, P.; Zeleňák, M. Turning of Wood Plastic Composites by Water Jet and Abrasive Water Jet. *Int. J. Adv. Manuf. Technol.* **2015**, *84*, 1615–1623. [CrossRef]

14. Kalirasu, S.; Rajini, N.; Rajesh, S.; Jappes, J.T.W.; Karuppasamy, K. AWJM Performance of Jute/Polyester Composite Using MOORA and Analytical Models. *Mater. Manuf. Process.* **2017**, *32*, 1730–1739. [CrossRef]

15. Pahuja, R.; Ramulu, M.; Hashish, M. Surface Quality and Kerf Width Prediction in Abrasive Water Jet Machining of Metal-Composite Stacks. *Compos. B Eng.* **2019**, *175*, 107134. [CrossRef]

16. Pahuja, R. Ramulu Abrasive Water Jet Machining of Titanium (Ti6Al4V)–CFRP Stacks–A Semi-Analytical Modeling Approach in the Prediction of Kerf Geometry. *J. Manuf. Process.* **2019**, *39*, 327–337. [CrossRef]

17. Hazir, E.; Ozcan, T. Response Surface Methodology Integrated with Desirability Function and Genetic Algorithm Approach for the Optimization of CNC Machining Parameters. *Arab. J. Sci. Eng.* **2019**, *44*, 2795–2809. [CrossRef]

18. Mirjalili, S. Moth-Flame Optimization Algorithm: A Novel Nature-Inspired Heuristic Paradigm. *Knowl. Based Syst.* **2015**, *89*, 228–249. [CrossRef]

19. Palleda, M. A Study of Taper Angles and Material Removal Rates of Drilled Holes in the Abrasive Water Jet Machining Process. *J. Mater. Process. Technol.* **2007**, *189*, 292–295. [CrossRef]

20. Mm, I.W.; Azmi, A.I.; Lee, C.C.; Mansor, A.F. Kerf Taper and Delamination Damage Minimization of FRP Hybrid Composites under Abrasive Water-Jet Machining. *Int. J. Adv. Manuf. Technol.* **2018**, *94*, 1727–1744. [CrossRef]

21. Kumar, D.; Gururaja, S. Abrasive Waterjet Machining of Ti/CFRP/Ti Laminate and Multi-Objective Optimization of the Process Parameters Using Response Surface Methodology. *J. Compos. Mater.* **2020**, *54*, 1741–1759. [CrossRef]

22. Rajamani, D.; Balasubramanian, E.; Murugan, A.; Tamilarasan, A. AWJC of NiTi Interleaved R-GO Embedded Carbon/Aramid Fibre Intermetallic Laminates: Experimental Investigations and Optimization through BMOA. *Mater. Manuf. Process.* **2023**, *38*, 1144–1158. [CrossRef]

23. Li, M.; Huang, M.; Yang, X.; Li, S.; Wei, K. Experimental Study on Hole Quality and Its Impact on Tensile Behavior Following Pure and Abrasive Waterjet Cutting of Plain Woven CFRP Laminates. *Int. J. Adv. Manuf. Technol.* **2018**, *99*, 2481–2490. [CrossRef]

24. Ciurana, J.; Arias, G.; Ozel, T. Neural Network Modeling and Particle Swarm Optimization (PSO) of Process Parameters in Pulsed Laser Micromachining of Hardened AISI H13 Steel. *Mater. Manuf. Process.* **2009**, *24*, 358–368. [CrossRef]

25. Ibrahim, M.A.; Çamur, H.; Savaş, M.A.; Abba, S.I. Optimization and Prediction of Tribological Behaviour of Filled Polyte-trafluoroethylene Composites Using Taguchi Deng and Hybrid Support Vector Regression Models. *Sci. Rep.* **2022**, *12*, 10393. [CrossRef]

26. Khalilpourazari, S.; Pasandideh, S.H.R. Multi-Objective Optimization of Multi-Item EOQ Model with Partial Backordering and Defective Batches and Stochastic Constraints Using MOWCA and MOGWO. *Oper. Res.* **2020**, *20*, 1729–1761. [CrossRef]

27. Khalilpourazari, S.; Naderi, B.; Khalilpourazary, S. Multi-Objective Stochastic Fractal Search: A Powerful Algorithm for Solving Complex Multi-Objective Optimization Problems. *Soft Comput.* **2020**, *24*, 3037–3066. [CrossRef]

28. Myszkowski, P.B.; Laszczyk, M. Diversity Based Selection for Many-Objective Evolutionary Optimisation Problems with Constraints. *Inf. Sci.* **2021**, *546*, 665–700. [CrossRef]
29. Devaraj, R.; Mahalingam, S.K.; Esakki, B.; Astarita, A.; Mirjalili, S. A Hybrid GA-ANFIS and F-Race Tuned Harmony Search Algorithm for Multi-Response Optimization of Non-Traditional Machining Process. *Expert Syst. Appl.* **2022**, *199*, 116965. [CrossRef]